Porous Flap Trailing Edges for the Reduction of Jet Installation Noise

Christian Jente[1], Jerome Huber[2], Celia Ekoule[2], Tristan Goffredi[3], Edoardo Paladini[3]

[1] *Deutsches Zentrum für Luft- und Raumfahrt e.V., 38108 Braunschweig, email: christian.jente@dlr.de*
[2] *AIRBUS Operations S.A.S., 31300 Toulouse, France*
[3] *Safran Aircraft Engines, 77550 Moissy Cramayel, France*

Introduction

Integrating modern jet engines under the wing of an existing aircraft platform is challenging: A number of constraints play various roles in the positioning of large-diameter aero engine between ground and wing. One of these constraints is the jet installation noise.

Experimental data was gathered from a small-scale wind tunnel test at the Aeroacoustic Wind Tunnel Braunschweig (AWB) in 2022. Two engine integration heights, i.e. the distance between the engine axis and the flap trailing edge, were tested. It can be shown that jet installation noise of the closer engine integration remains nearly the same when the flap is partially equipped with porous noise reduction technology (NRT).

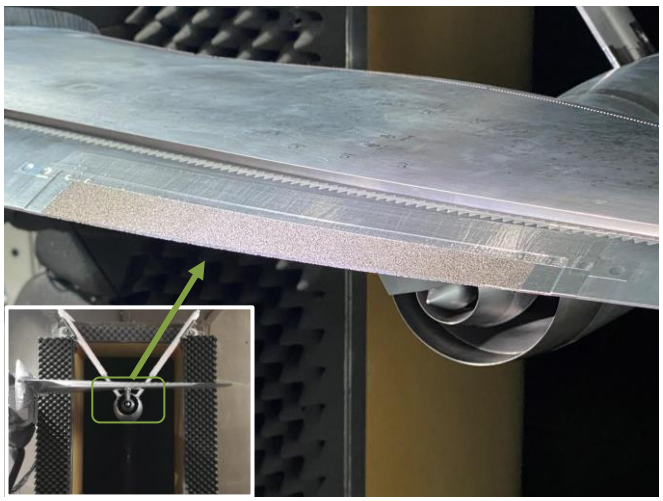

Figure 1: Porous flap insert at AIRBUS RDJ80 wing and pylon-mounted SAFRAN UHBR engine at AWB wind tunnel test, October 2022.
AIRBUS DLR SAFRAN proprietary data.

Test facility and experimental setup

AWB is a closed-circuit wind tunnel with a rectangular wind tunnel nozzle (ΔY=0.8m x ΔZ=1.2m), an open test section (ΔX~3.6m) and wind tunnel velocities of up to 60 m/s.

The **SAFRAN engine model** is a dual stream short cowl UHBR engine with a bypass-to-core area ratio of ~7, and a mixed jet diameter of D_{mix} close to 100mm. Bypass and core engine were operated at equal velocity, achieving several same speed jet operations in between 145…295m/s (Figure 2). The reference operation for figures 6 and 8 is the flight operation OP6|60, i.e. jet velocity of 244m/s and wind tunnel velocity of 60m/s.

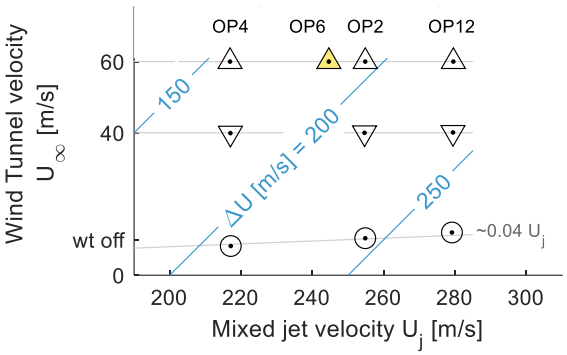

Figure 2: Test operations chart. The installed jet configurations have been tested for the static and flight operations.

The **AIRBUS RDJ80_1-wing** is a right-hand (starboard-side) half model with a chord length of 300mm in the engine integration plane. The two-element wing consists of its main wing and the flap which are both tripped on pressure side and suction side. Some flap parameters can be adjusted: the flap deflection angle, here δ_F=14°, via brackets and the material property by an exchangeable mid-section:

There is the AIRBUS baseline flap made of solid material, and the DLR flap which contains a porous insert. A major step towards technology readiness is the successful manufacture of the geometrically complex 3D geometry via electric discharge machining. The insert is characterized by a span width of 300mm (~3 mixed jet diameters) and covers less than half (42%) of the flap chord length (Figures 1 and 3).

The porous material has been selected to resemble the porous aluminum PA80-110 [1]. The raw material is produced by casting an aluminum alloy onto crystal salt particles with grain size 80-110µm. After washing, the surfaces are permeable with an open pore size of 400 - 1000µm according to the manufacturer.

The material showed promising noise reduction potential in an installed jet pre-test at DLR-JExTRA in Berlin [2]. However, the test was limit to static operations only, while noise reduction at flight operations remained to be investigated. This gap was closed with the AWB test and key results are published in this paper.

The engine is integrated under the wing via a pylon model. The presence of the pylon decreases the bypass outlet area and causes asymmetry in the jet.

The **engine integration** length between bypass nozzle outlet and flap trailing edge is L =2.77 D_{mix} (see Figure 3).

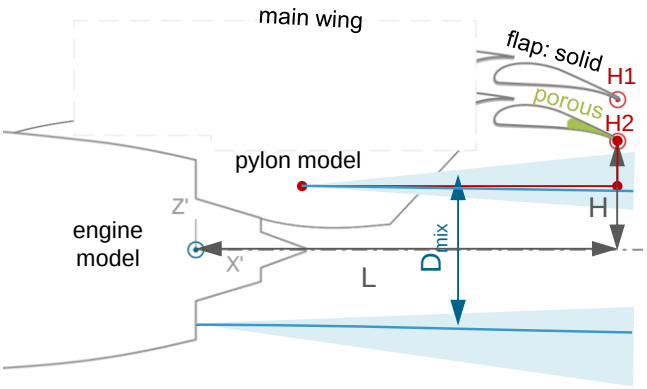

Figure 3: Engine integration parameters of H_1 installation vs. H_2 w/ porous flap insert at engine symmetry plane.

Starting from the reference engine integration height of H_1 ~ 0.98 D_{mix}, the installation penalty of the closer coupling H_2 ~0.71 D_{mix} is determined and attempted to be eliminated with help of the porous NRT.

Instrumentation

The flyover arc under the model is instrumented with a DLR Berlin line array (see Figures 4 and 5).

The distance between the engine axis and the line array is R=1.78m, which is a rather close geometric distance (R/D_{mix}=17.8) for jet-related problems [3].

The polar arc is resolved by 47x ¼" MK301 microphones (Microtech Gefell) in between aft-to-front installation angles of 50° to 134° w.r.t. x = flap trailing edge and z = engine axis (Figure 5).

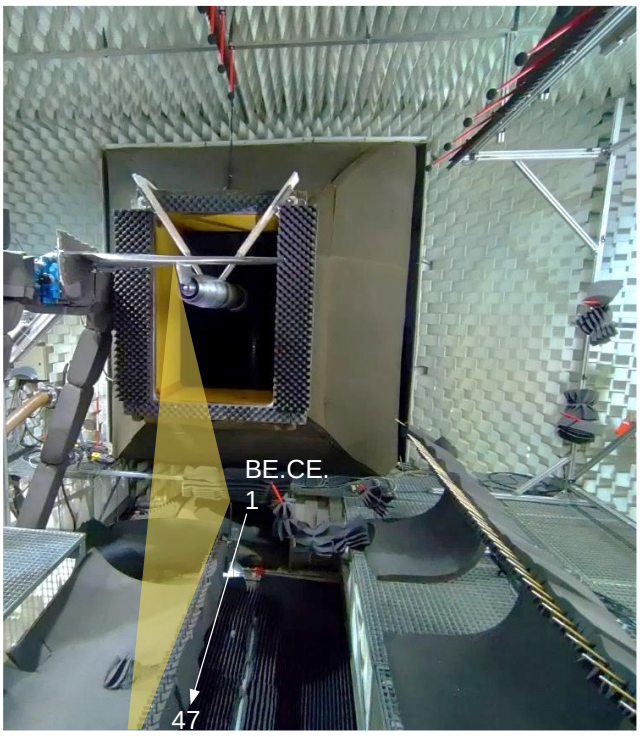

Figure 4: DLR-Berlin Flyover Array w/ 47 ¼" mics installed at the bottom of AWB.
AIRBUS DLR SAFRAN proprietary data.

Jet installation effect along the flyover arc

The first evaluation is to determine the Overall Sound Pressure Level (OASPL) at each microphone position by energetic addition of one-third octave gains in the frequency range between 630Hz (He=0.5) and 20kHz (He=16).

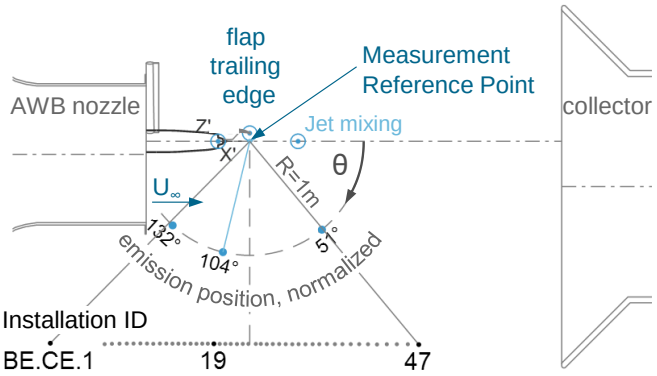

Figure 5: Microphone positions along the flyover arc of the open test section in AWB.

The installation effect is calculated by arithmetically subtracting the isolated jet noise from the installed jet noise (Equation 1).

$$\Delta OASPL = OASPL_{inst} - OASPL_{iso} \quad [\text{dB}] \quad (1)$$

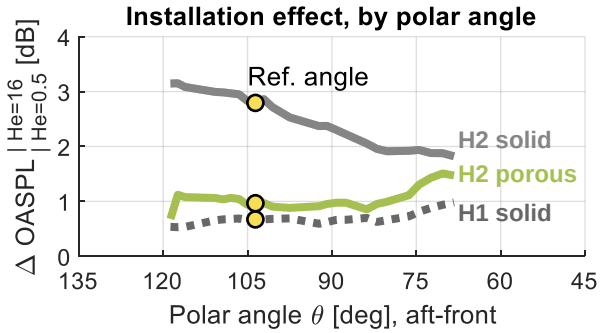

Figure 6: Jet installation effect, i.e. difference between installed and isolated build, along flyover arc for flight OP6|60, i.e. jet at 244 m/s and wind tunnel at 60 m/s.

The reference engine integration at H_1 causes an installation effect of nearly 1dB (dotted gray line in Figure 6) along the measured arc. While the closer coupling at H_2 causes an installation penalty of nearly 3dB (gray line), the porous insert (green line) helps to keep the installation effect within 1 to 1.5dB.

This means that the porous insert helps to almost completely eliminate the additional installation penalty.

DLR conducted the following analysis on velocity and jet installation noise frequencies, selecting a microphone (θ=104°, i.e. perpendicular to the deflected flap) with a particularly high signal.

Velocity sensitivity and scaling laws

OASPLs for different operations are compared against each other. The shear layer difference velocity (Equation~2, Figure 2) between the wind tunnel flow and the (bypass) jet was found to be a suitable scaling parameter.

$$\Delta U = U_j - U_\infty \qquad \text{[m/s]} \qquad (2)$$

The lower diagram of Figure 7 shows the before defined installation effect (Equation 1). The reference operation is representative for the installation effect and NRT performance at other operations. However, the installation effect is slightly larger for low ΔU.

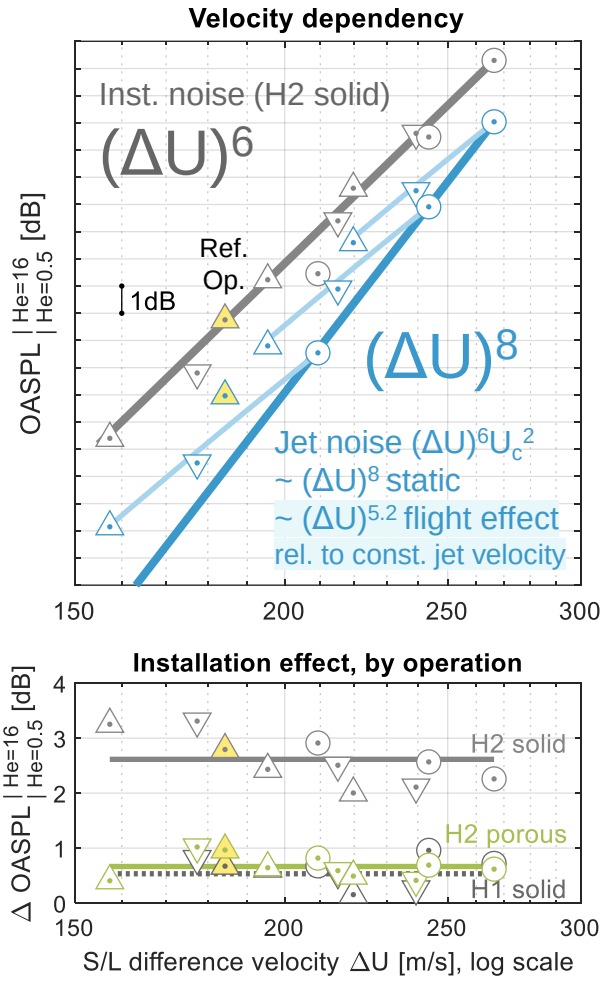

Figure 7: Upper part: velocity scaling laws for isolated jet and installed setting (H2 solid). Lower part: Installation effect depending on shear layer difference velocity at reference polar angle θ=104°.

This can be explained with velocity scaling exponents depicted in the upper part of Figure 7. As both axes, OASPL and ΔU, are logarithmic, velocity scaling exponents can be identified by the slope of the data points:

- Static jet noise data points (dark blue) follow the eighth power analogy derived by Lighthill.
- Flight jet noise data points collapse within a 1-2dB band of the same eight power line. Acoustic analogies tailored to flight jet noise [4] derive a fifth to sixth power collapse w.r.t. the corresponding static jet operation (light blue).
- Jet installation noise (here H_1 solid) collapses well with the sixth power of ΔU. This scaling exponent is an indicator of loading noise.

Jet installation noise by frequency

Which frequencies are particularly contributing to the installation noise? - Since OASPL is calculated from one-third octave SPL, the y-axis of Figure 8 shows one-third octave data (bright colors). In addition, narrowband data is plotted to rule out any interpretation errors due to strong tones [5]. This is done by plotting "$PSD \cdot f$", with decibel levels according to Equation 3, in order to achieve the same shape as the one-third octave band's one.

$$\underbrace{SPL_{nb} - 10\lg(\Delta f_{nb})}_{PSD} + 10\lg(\Delta f_{1/3}) \qquad \text{[dB]} \qquad (3)$$

The velocity scaling exponents indicate that the installation noise is driven by the compactness of the wing w.r.t. the jet, which is why Helmholtz number is here chosen as the dimensionless frequency (Equation 4), where a_∞ is the speed of sound and L is the engine integration length.

$$He_L = \frac{f \cdot L}{a_\infty} \qquad \text{[-]} \qquad (4)$$

The following three frequency regions can be distinguished:

III. He>1: There is only a small and almost constant offset w.r.t. the reference jet noise, especially for He>4. Wavepackets of envelopes lower than L reflect off the pressure side of the wing surface.

I. He<1: Pressure fluctuations with wavelengths greater than L produce low frequency excess noise on the wing pressure side. Once they reach a singularity, i.e. the trailing edge, they are scattered into the far-field.

Jet-flap interaction

II. He=1: Wavelengths of dimension L cause feedback between flap trailing edge and jet shear layer origin. This effect is particularly large when the flap is forced to interact with the jet shear layer and rather insignificant for large H (e.g. see H_1).

Isolated jet noise cross-comparison

An isolated jet noise cross-comparison is used to assess the data quality. This is not straight-forward, since the isolated engine features a pylon and produces a slightly non-symmetric and deflected jet.

Nevertheless, this dual-stream jet noise compares well to a round single stream jet (NASA SJET model [6]) for frequencies above He=0.5 when applying a 1dB offset (see blue curves in Figure 8).

Yet, this is not the case for Helmholtz numbers He<0.5. Since the pylon does not seem to influence low frequency jet noise [7], the isolated jet noise is likely to be corrupted, albeit for arguably low frequencies, i.e. Sr_{mix}<0.3.

Three factors support the argument that facility noise also affects the installation noise in frequency band I: (1) The unexpected (see [8], [9]) minimal gain decrease between the H_1 and H_2 (solid) setups, and (2) the comparably poor porous NRT performance (see [2], [10]) at very low frequencies. (3) The source localization (not shown) by DLR-B and ONERA also identifies excess noise which originates downstream the test section and the AWB collector.

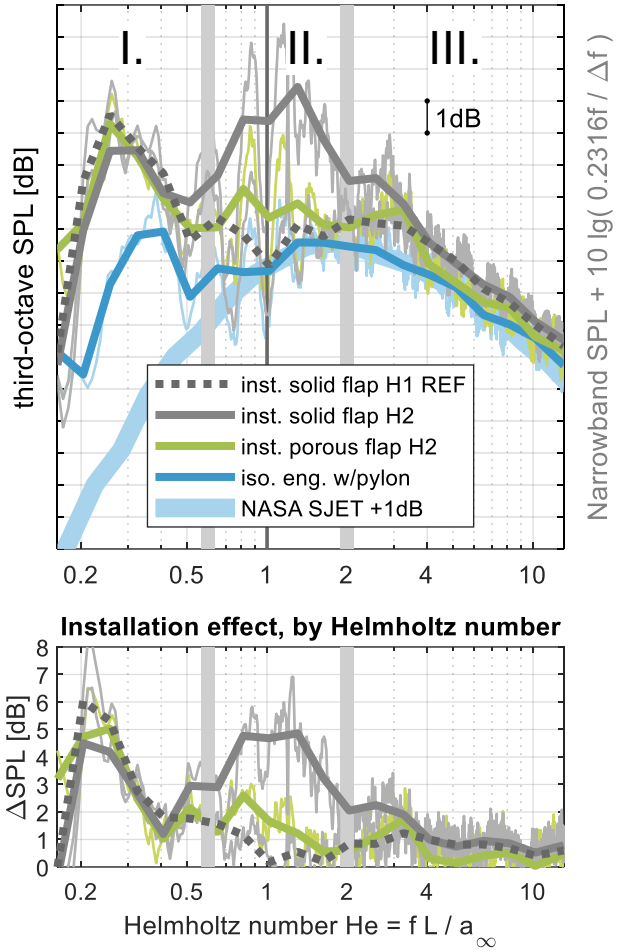

Figure 8: Upper part: third-octave band spectra by Helmholtz number (operations: jet at 244 m/s, WT 60 m/s, reference polar angle 104°). Lower part: Installation effect, i.e. installed – isolated noise.

Summary and Outlook

By compensating additional jet installation noise at a tighter engine integration, the porous flap trailing edge technology helps to mitigate the jet installation noise back to the noise level of a moderately-coupled configuration. The height difference of $\Delta H = 0.27\ D_{mix}$ is comparable to more than half of the ground clearance of a typical commercial airliner.

Future research will focus on optimizing porous material properties (e.g. graded material, see NRT3 in [2]) and geometry (optimal porous span and chord length) and on tackling other technology readiness related challenges.

Acknowledgements

Special thanks to A. Markesteijn (QMUL) for generating NASA SJET reference data w/permission, the extended AWB test and analysis team, including H. Siller, W. Hage, A. Bassetti (DLR Berlin) and H. Demontis (ONERA).

The EU DJINN (Decrease Jet Installation Noise) project receives funding from the European Union's Horizon 2020 research and innovation programme under grant agreement No 861438. DJINN is a collaborative effort between CFD-Berlin (coordinator), Airbus SAS, Dassault Aviation, Safran Aircraft Engines, Rolls-Royce Deutschland, ONERA, DLR, University of Southampton, CERFACS, Imperial College London, von Karman Institute, CNRS, and Queen Mary University of London (QMUL).

Literature

[1] Herr, M., Rossignol, K.-S., Delfs, J., Lippitz, N., and Mößner, M., Specification of Porous Materials for Low-Noise Trailing-Edge Applications. 20th AIAA/CEAS Aeroacoustics Conference, 2014, DOI: 10.2514/6.2014-3041

[2] Jente, C., Schmidt, J., Delfs, J., Rossignol, K-S, Pott-Pollenske, M., Siller, H., Noise reduction potential of flow permeable materials for jet-flap interaction noise, 28th AIAA/CEAS Aeroacoustics Conference, 2022. DOI: 10.2514/6.2022-3040, see NRT4 and NRT3

[3] Viswanathan K. Best Practices for Accurate Measurement of Pure Jet Noise. International Journal of Aeroacoustics. 2010; 9(1-2): 145-206. DOI: 10.1260/1475-472X.9.1-2.145, see p.203

[4] Michalke, A. and Michel, U., Prediction of jet noise in flight from static tests, Journal of Sound and Vibration, Vol. 67, No. 3, 1979, pp. 341-367. DOI: 10.1016/0022-460X(79)90541-8, eqn 4.31

[5] Jordan, P., Jaunet, V., Towne, A., Cavalieri, A. V. G., Colonius, T., Schmidt, O., and Agarwal, A., Jet-flap interaction tones, Journal of Fluid Mechanics, Vol. 853, 2018, pp. 333-358. DOI: 10.1017/jfm.2018.566

[6] Khavaran, A., Bridges, J.: SHJAR Jet Noise Data and Power Spectral Laws. Technical Report NASA/TM 2009-215608 (2009)

[7] Faranosov, G., Kopiev, V., Ostrikov, N., Kopiev, V.A., The effect of pylon on the excess jet-flap interaction noise, 22nd AIAA/CEAS Aeroacoustics Conference, 2016, DOI: 10.2514/6.2016-3043, i.a. fig.7-9

[8] Mengle, V., The Effect of Nozzle-to-Wing Gulley Height on Jet Flow Attachment to the Wing and Jet-Flap Interaction Noise, 17th AIAA/CEAS Aeroacoustics Conference, 2011, DOI 10.2514/6.2011-2705, fig.8

[9] Lawrence, J., Azarpeyvand, M., Self, R., Interaction between a Flat Plate and a Circular Subsonic Jet, 17th AIAA/CEAS Aeroacoustics Conference, 2011, DOI 10.2514/6.2011-2745, fig.6

[10] Rego, L., Ragni, D., Avallone, F., Casalino, D., Zamponi, R., Schram, C., Jet-installation noise reduction with flow-permeable materials, JSV 2021, DOI: 10.1016/j.jsv.2021.115959